Intracranial Artery Morphology in Pediatric Moya Moya Disease and Moya Moya Syndrome

Vivek S. Yedavalli, MD [‡*]
Jennifer L. Quon, MD [§*]
Elizabeth Tong, MD [‖]
Eric K. van Staalduinen, DO [¶]
Pauline Mouches, MSc [¶]
Lily H. Kim, MD [§]
Gary K. Steinberg, MD, PhD [§]
Gerald A. Grant, MD [§]
Kristen W. Yeom, MD [‖]
Nils D. Forkert, PhD [¶]

[‡]Department of Radiology and Radiological Sciences, Johns Hopkins School of Medicine, Baltimore, Maryland, USA; [§]Department of Neurosurgery, Stanford University School of Medicine, Palo Alto, California, USA; [‖]Department of Radiology, Stanford University School of Medicine, Palo Alto, California, USA; [¶]Department of Radiology, Alberta Children's Hospital Research Institute, University of Calgary, Calgary, Alberta, Canada

*Vivek S. Yedavalli and Jennifer L. Quon contributed equally to this work.

Correspondence:
Vivek S. Yedavalli, MD,
Department of Radiology and Radiological Sciences,
Johns Hopkins University School of Medicine,
Phipps Building B112-D,
Baltimore, MD 21287, USA.
Email: vyedava1@jhmi.edu

Received, January 25, 2022.
Accepted, June 5, 2022.
Published Online, August 22, 2022.

BACKGROUND: Moya Moya disease (MMD) and Moya Moya syndrome (MMS) are cerebrovascular disorders, which affect the internal carotid arteries (ICAs). Diagnosis and surveillance of MMD/MMS in children mostly rely on qualitative evaluation of vascular imaging, especially MR angiography (MRA).

OBJECTIVE: To quantitatively characterize arterial differences in pediatric patients with MMD/MMS compared with normal controls.

METHODS: MRA data sets from 17 presurgery MMD/MMS (10M/7F, mean age = 10.0 years) patients were retrospectively collected and compared with MRA data sets of 98 children with normal vessel morphology (49 male patients; mean age = 10.6 years). Using a level set segmentation method with anisotropic energy weights, the cerebral arteries were automatically extracted and used to compute the radius of the ICA, middle cerebral artery (MCA), anterior cerebral artery (ACA), posterior cerebral artery (PCA), and basilar artery (BA). Moreover, the density and the average radius of all arteries in the MCA, ACA, and PCA flow territories were quantified.

RESULTS: Statistical analysis revealed significant differences comparing children with MMD/MMS and those with normal vasculature ($P < .001$), whereas post hoc analyses identified significantly smaller radii of the ICA, MCA-M1, MCA-M2, and ACA ($P < .001$) in the MMD/MMS group. No significant differences were found for the radii of the PCA and BA or any artery density and average artery radius measurement in the flow territories ($P > .05$).

CONCLUSION: His study describes the results of an automatic approach for quantitative characterization of the cerebrovascular system in patients with MMD/MMS with promising preliminary results for quantitative surveillance in pediatric MMD/MMS management.

KEY WORDS: Moya Moya disease, MR angiography, Vessel morphology, Brain development

Neurosurgery 91:710–716, 2022 https://doi.org/10.1227/neu.0000000000002099

Moya Moya disease (MMD) is a progressive, noninflammatory vasculopathy characterized by steno-occlusive disease of the anterior circle of Willis (COW), comprising the distal internal carotid arteries (ICAs), proximal middle cerebral arteries (MCAs), and proximal anterior cerebral arteries (ACAs).[1] It is assumed that collateralization of perforator branches develops as a compensatory mechanism secondary to the reduced blood flow caused by the steno-occlusive disease, leading to the "puff of smoke" appearance on digital subtraction angiography (DSA).[2] By contrast, Moya Moya syndrome (MMS) is distinct from the disease itself, where an underlying etiology leads to a COW steno-occlusive disease similar in appearance to MMD.[1] The most common etiologies of MMS include atherosclerosis, radiation-related vasculitides, connective tissue disorders, and phakomatoses.[2]

Although DSA is considered the gold standard for MMD/MMS diagnosis, MR angiography (MRA) is a widely accepted noninvasive alternative.[3] However, imaging diagnosis of pediatric MMD/MMS to date is primarily qualitative because quantitative normative vessel calibers and densities across childhood have only been characterized and described recently.[4] Therefore, previously described quantitative methods for evaluating MMD/MMS are limited to brain tissue measurements including cerebral blood flow[5] or metrics computed from diffusion-weighted imaging, such as the apparent diffusion coefficient.[6] Quantitative MRA-based analyses of

ABBREVIATIONS: BA, basilar artery; **COW,** circle of Willis; **MANCOVA,** multivariate analysis of covariance; **MMD,** Moya Moya disease; **MMS,** Moya Moya syndrome; **MNI,** Montreal Neurological Institute; **MRA,** MR angiography; **PCA,** posterior cerebral artery; **TOF,** time-of-flight.

the arteries to date have primarily focused on healthy adults[7,8] with unclear potential for pediatric patients with MMD/MMS. Given that MRA can be acquired without contrast agent, radiation, and in many children even without sedation, quantitative approaches for evaluating the cerebrovascular system based on MRA are particularly desirable and an important step toward precision medicine.[9]

The aim of this study was to identify differences in artery caliber and density between children with MMD/MMS and children with normal vasculature based on MRA data sets using recently described normative quantitative cerebral artery parameters across childhood.[4]

METHODS

Patients

Pediatric patients with MMD/MMS vessel morphology admitted at our institution between 2011 and 2018 were retrospectively identified using chart review. Only patients with available MRI and time-of-flight (TOF) MRA data sets were included (a total of 233 consecutive patients with MMD/MMS were identified). Next, children who received bypass surgery before imaging and children with any prior hemorrhage were excluded due to the associated blood flow alterations, resulting in 33 patients with MDD/MMS. Finally, all data sets (n = 16) with motion artefacts and patients with insufficient registration or segmentation results were excluded leading to a total final set of 17 data sets available for this study. The age of the included patients with MDD/MMS ranged from 2.4 to 18 years (mean ∅ = 10.0 years), with 10 male patients (∅ = 10.3 years) and 7 female patients (∅ = 9.6 years). Eleven children had bilateral disease while 6 children had unilateral disease only (3 left and 3 right) (please see Table 1).

The normal control cohort used for comparison contained data sets from 98 consecutive patients with normal MRA examinations and no known neurological deficits or developmental problems, imaged using similar imaging parameters on the same scanner as the patient cohort (49 female patients, 49 male patients, ∅ = 10.6 years, range 0.5-20 years). Reasons for imaging in this normal cohort included, for example, headaches, transient but resolved neurological symptoms, strabismus, or family history of vascular malformations. The normal control group used for this study is described in detail elsewhere.[4]

This retrospective study was conducted in compliance with the Health Insurance Portability and Accountability Act and in accordance with the ethical standards laid down in the 1964 Declaration of Helsinki and its later amendments after Institutional Review Board approval. Patient consent was waived given the retrospective nature of this study.

Image Acquisition

All data sets were acquired on the same 3-dimensional (3D) MRI scanner. High-resolution T1-weighted MRI and time-of-flight MRA data sets were acquired for each patient on a 3T Discovery 750 scanner (GE Medical Systems) using an 8-channel head coil. High-resolution TOF MRA was acquired using an echo time (TE) of 3.2 ms, a repetition time (TR) of 24 ms, a flip angle of 15°, and a spatial resolution of 0.43 × 0.43 × 0.6 mm³. The high-resolution T1-weighted data sets were acquired with TE = 3.5 ms, TR = 7.8 ms, inversion time (TI) = 400 ms, flip angle = 15°, and a spatial resolution of 0.47 × 0.47 × 1.0 mm³ in a single 175 slice slab. At our institution, intravenous propofol sedation is typically performed for all children younger than 6 years. After 10 years of age, generally no patient receives sedation.

Image Processing

The image-processing pipeline used in this study follows that previously described by Ratsep et al,[10] briefly described in the following. The full pipeline is fully automatic and does not require any manual interaction making its quantitative results robust and comparable.

First, the MRA data sets were preprocessed using an algorithm[11] to remove slice-wise intensity variations followed by application of the N3 algorithm[12] to correct for in-slice intensity inhomogeneities. Next, the arteries were automatically segmented in each MRA data set using an advanced level set algorithm with anisotropic energy weights.[13] The resulting segmentations were used to quantify the local vessel radii by calculating the 3D centerline representations of the vascular segmentations[14] followed by a 3D distance map calculation[15] to determine the shortest Euclidean distance from each centerline voxel to its closest nonvessel voxel.

For quantitative analysis at corresponding locations, the Montreal Neurological Institute (MNI) average 152 subject adult brain atlas was registered nonlinearly to the MNI pediatric atlas (7-11 years),[16] which was then registered nonlinearly to each T1-weighted data set. In the next step, the patient-individual T1-weighted data set was registered rigidly to the corresponding MRA data set of each patient. Finally, the 3 transformations were concatenated and used to transform regions-of-interest (ROI) defined in the adult MNI brain atlas to each subject-specific MRA data set. The NiftyReg software[17] was used for all registrations described above. All segmentations and registrations were visually checked by an experienced imaging specialist with dedicated experience in cerebral vessel analysis (NDF, >10 years' experience). Patients with suboptimal processing results and those with severe imaging artifacts were excluded.

Artery Quantification

The concatenated transform resulting from the registration was used to map vascular flow territory atlas regions defined in MNI atlas space[18] to each MRA data set. This flow territory atlas consists of the left and right ACA, MCA, and posterior cerebral artery (PCA) flow territories, whereas the proximal, middle, and distal parts for each territory were combined to a single region-of-interest (ROI). Using these 6 flow territory ROIs, the artery density and average artery radius were quantified for each territory and hemisphere. For the average flow territory artery radius, only radius values of centerline voxels were averaged to prevent large vessels having a higher weight in the computed average value. The artery density was quantified for each flow territory by calculating the ratio between the volume of segmented arteries and the volume of the whole flow territory.

Finally, the radius of the 5 main arteries were quantified by using corresponding artery ROIs defined in the MNI atlas space[19] mapped to each individual MRA data set using the concatenated transformation described above. The arteries investigated included the ICA, ACA, MCA (M1 and M2 segments), the basilar artery (BA), and the PCA (Figure 1). All main artery measurements were performed separately for the left and right hemisphere except for the BA, which is a single artery, and the ACA, which can be challenging to quantify automatically separately for the 2 hemispheres because of the close proximity so that the corresponding ROI includes both arteries.

Qualitative Analysis

Qualitative analyses were independently performed in addition to the previously described quantitative analyses. Qualitative analyses of the MMD/MMS and normal subgroup MRA data sets were performed by a pediatric neuroradiologist (Kristen W. Yeom, 20 years' experience). Therefore, the overall vessel density and the vessel diameters at

TABLE 1. Baseline Characteristics of Each Subgroup

Characteristic	MMD/MMS	Control
Number of patients	33	98
Mean age (y)	10.0 (2.4-18)	10.6 (0.5-20)
Female patients	7	49
Race		NA
White	16	
Hispanic	7	
Black	4	
Asian	4	
Mixed Asian/White	2	
Bilateral disease	11	NA
Unilateral disease	6	NA
MMD	7	NA
MMS		
Trisomy 21	7	
Neurofibromatosis 1	3	
Sickle cell	4	
Other (TSC1, PHACES, DiGeorge, Dwarfism, etc)	12	

MMD, Moya Moya disease; MMS, Moya Moya syndrome; PHACES, posterior fossa anomalies, hemangioma, arterial anomalies, cardiac anomalies, and eye anomalies; TSC1, Tuberous Sclerosis Complex 1.

corresponding locations were visually assessed to identify relevant differences between the groups.

Statistical Analysis

Multivariate analysis of covariance (MANCOVA) was used to compare the MMD/MMS and normal cohorts using the radius of the 5 main arteries as well as the average artery radius and density measurements from the flow territories as dependent variables, age and sex as covariates, and the group (normal vs MMD/MMS) as the fixed factor. MANCOVA tests were performed separately for left and right hemispheric measurements, whereas only patients with left unilateral or bilateral MMD/MMS were used for the MANCOVA of the left hemispheric measurements while only patients with right unilateral or bilateral MMD/MMS were used for the MANCOVA of the right hemispheric measurements. The BA and ACA radius measurements were included in both MANCOVA tests (left and right hemispheric measurements).

Pairwise comparisons of the dependent variables with Bonferroni correction were performed post hoc to identify significant parameters. IBM SPSS Statistics (v24.0, IBM) was used for all analyses. A Bonferroni-corrected $P < .004$ was considered significant for the post hoc tests while $P < .025$ was considered significant for the MANCOVA analysis.

RESULTS

Qualitative Analyses

Visual analysis of the quantitative artery analysis showed considerably larger arteries in the anterior circulation while the overall density of vessels and size of the smaller vessel seemed comparable between MMD/MMS (presurgery) and healthy children. Figure 2 shows 2 representative patients with MMD/MMS and 2 age-matched normal subjects for comparison purposes. In these examples, the healthy children display larger ICA and MCA M1 vessels compared with patients with MMD/MMS indicated by warmer colors. By contrast, the overall vessel density and radius of the smaller vessels in the downstream branches seem similar in the 2 groups as indicated by a similar color pattern.

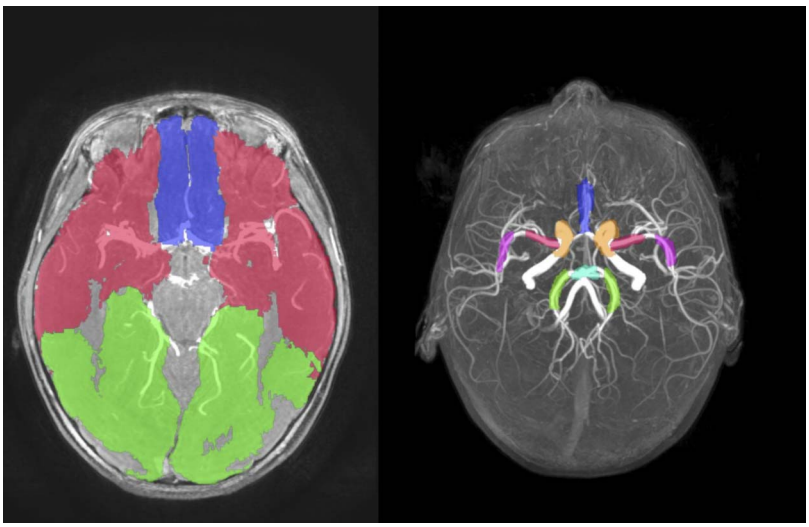

FIGURE 1. *MCA (red), ACA (blue), and PCA (green) flow territories (left) and internal carotid artery (orange), MCA-M1 (red), MCA-M2 (purple), ACA (blue), basilar artery (turquoise), and PCA (green) regions of interest (right). ACA, anterior cerebral arteries; MCA, middle cerebral artery; PCA, posterior cerebral artery.*

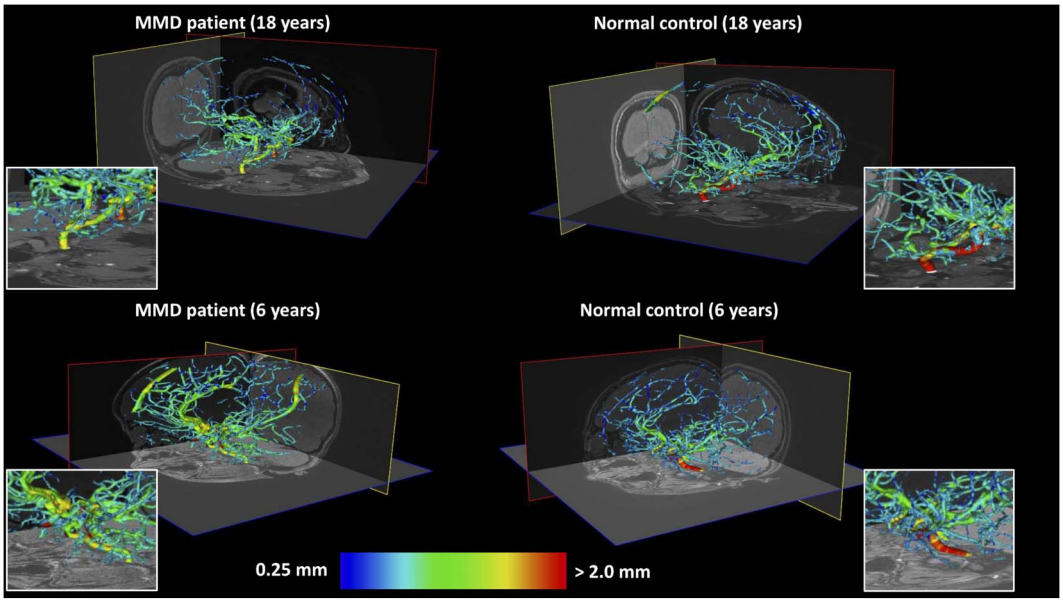

FIGURE 2. *3D surface-based visualizations of 2 children with MMD (left) and 2 corresponding age-matched children with normal cerebrovascular system (right). 3D, 3-dimensional; MMD, Moya Moya disease.*

Quantitative Analyses

The statistical analysis using MANCOVA support the qualitative findings, revealing a statistically significant difference between the MMD/MMS (presurgery) and normal cohorts, which holds true for left and right hemispheric measurements ($P < .001$ in both cases). Pairwise comparisons revealed significant differences of the radius measurements in all major arteries of the anterior circulation investigated, comprising ICA, MCA-M1, MCA-M2, and ACA radii ($P < .001$, left and right). However, no significant differences were found for the pairwise comparisons of the posterior circulation vasculature, any mean flow territory artery radius, or any flow territory artery density after correction for multiple testing (Table 2).

DISCUSSION

Quantitative assessment of morphological vessel characteristics can yield objective information that facilitates standardization and reduce observer variability.[20] Vessel caliber and density quantification in MMD/MMS and normal pediatric cohorts are therefore essential for standardization of image-based biomarkers and are potentially valuable for surveillance. This work presents the first report of a quantitative vessel caliber and density analysis for pediatric patients with MMD/MMS. The main finding of this study is that children with MMD/MMS before surgery showed significantly smaller main anterior circulation arteries while the overall vessel density and caliber in the 3 flow territories were similar compared with healthy children.

The finding that children with MMD/MMS have smaller main arteries in the anterior circulation compared with normal children likely reflects an early stage of MMD/MMS with predominantly anterior arterial steno-occlusion that comprised our pediatric cohort because the posterior circulation pathology has a later onset in disease progression.[21,22] Previous studies have also shown that patients with MMD/MMS have diminished vessel caliber. For example, Yamamoto et al[23] demonstrated not only smaller arteries (ICA, MCA, and ACA) at the initial MMD stages but also spontaneous progression over time in 7 adult and pediatric patients with MMD leading to further diminished vessel caliber. This finding was reproduced in other adult[24-28] and children[28-30] studies using qualitative assessments. Our results are consistent with those previous reports, with the novel addition of a robust and automatic quantification and a comparably large pediatric patient cohort. We also showed that the smaller artery caliber in patients with MMD/MMS primarily affects the main arteries while the average artery caliber within the 3 flow territories is similar to healthy children. One potential explanation for this finding might be that the MRA spatial resolution prevents the precise quantification of subtle radius differences in smaller arteries. Another possible explanation might be a gradual compensatory neoangiogenesis reactively formed because of the small caliber proximal vasculature to maintain cerebral blood flow.

Previous clinical studies investigating vessel density are rather sparse. For instance, Czabanka et al[31] found increased microvascular density in 16 adult patients with MMD when compared with separate atherosclerotic disease and normal control cohorts. Contrary, no significant differences regarding the vessel density in the flow territories were found in this study. This discordance may

TABLE 2. Age-Corrected and Sex-Corrected Average Artery Measurements (± SE) for Pediatric Patients With MMS/MMD and the Normal Control Group

Arterial vessel	MMD/MMS patients	Normal controls	*P* value
Main artery radius			
Left ICA radius (in mm)	1.197 ± 0.091	1.615 ± 0.034	**<.001**
Right ICA radius (in mm)	1.145 ± 0.094	1.659 ± 0.035	**<.001**
Left MCA M1 radius (in mm)	0.832 ± 0.045	1.146 ± 0.017	**<.001**
Right MCA M1 radius (in mm)	0.825 ± 0.043	1.148 ± 0.016	**<.001**
Left MCA M2 radius (in mm)	0.615 ± 0.041	0.831 ± 0.015	**<.001**
Right MCA M2 radius (in mm)	0.629 ± 0.038	0.816 ± 0.014	**<.001**
ACA radius (in mm)	0.659 ± 0.039	0.836 ± 0.015	**<.001**
BA radius (in mm)	1.090 ± 0.052	1.130 ± 0.020	.476
Left PCA radius (in mm)	0.840 ± 0.036	0.854 ± 0.014	.722
Right PCA radius (in mm)	0.883 ± 0.039	0.854 ± 0.015	.490
Average flow territory artery radius			
Left MCA flow territory radius (in mm)	0.603 ± 0.010	0.582 ± 0.004	.047
Right MCA flow territory radius (in mm)	0.610 ± 0.009	0.595 ± 0.004	.125
Left ACA flow territory radius (in mm)	0.577 ± 0.010	0.582 ± 0.004	.659
Right ACA flow territory radius (in mm)	0.614 ± 0.014	0.586 ± 0.005	.072
Left PCA flow territory radius (in mm)	0.593 ± 0.013	0.581 ± 0.005	.399
Right PCA flow territory radius (in mm)	0.606 ± 0.018	0.608 ± 0.007	.916
Average flow territory artery density			
Left MCA flow territory density (in %)	0.725 ± 0.090	0.682 ± 0.034	.653
Right MCA flow territory density (in %)	0.616 ± 0.078	0.643 ± 0.030	.749
Left ACA flow territory density (in %)	0.703 ± 0.096	0.588 ± 0.036	.264
Right ACA flow territory density (in %)	0.898 ± 0.115	0.813 ± 0.043	.492
Left PCA flow territory density (in %)	1.138 ± 0.150	0.893 ± 0.057	.129
Right PCA flow territory density (in %)	1.199 ± 0.189	1.040 ± 0.071	.435

ACA, anterior cerebral arteries; BA, basilar artery; ICA, internal carotid artery; MCA, middle cerebral artery; MMD, Moya Moya disease; MMS, Moya Moya syndrome; PCA, posterior cerebral artery.
P values < .004 were considered significant (Bonferroni corrected).
Bolded terms are statistically significant.

be explained by physiological differences between pediatric and adult MMD/MMS[32] with pediatric patients with MMD, for example, exhibiting increased oxygen extraction fraction.[33] Therefore, the discordance regarding vessel density may be explained by the presence of robust collaterals during the nascent stages of the disease in the pediatric population, which then maintains the blood flow and perfusion pressure through the comparatively increased oxygen extraction fraction. This physiological response may be sufficient, effectively decreasing the need for neovascularization and a compensatory increase in flow territorial vessel density. However, it needs to be highlighted that it was not possible to adequately analyze the microvascular density in this study in more detail because of the MRA spatial resolution. Thus, it is also possible that while the microvascular density differs between patients with MMS/MMS and normal subjects, the macrovascular density is similar.

Limitations

There are several limitations to this study. First, our study was based on a relatively small number data sets. Given the rarity of MMD/MMS, it was challenging to identify children with sufficient quality data sets for automatic vessel analyses. A pediatric neuroradiologist performed extensive quality control to prevent artifacts or any secondary pathologies affecting the MMD vessel evaluation. Furthermore, all data sets were acquired at a single institution imaged with the same MRI scanner, potentially limiting generalizability. As described above, the MRA spatial resolution may limit the accuracy of the small vessel measurements. Nevertheless, the significant differences found comparing the major arteries between the groups should be less affected by the spatial resolution so that those results will likely hold true in case of imaging with higher spatial resolution. We did not compare our results to the reference standard DSA. DSA is typically acquired with anteroposterior and lateral projections only and in a dynamic fashion, which makes it challenging to measure the same locations in DSA and MRA. Moreover, not all the subjects had corresponding DSA imaging, while in other cases, both image modalities were acquired with considerable time difference, which may bias a comparison. For those reasons, no comparison was performed for this study, which should be investigated in future. Owing to the small sample size, it was not possible to compare the artery measurements between the patients with MMD and MMS and investigate whether any image-

based biomarker differentiate the 2 groups. Although it cannot be ruled out that propofol affects the artery radius measurements, a previous study did not find any differences for the cerebral blood flow comparing healthy children with and without propofol sedation.[34] Owing to the relation of brain tissue perfusion and macrovascular blood flow, the effect of propofol on artery measurements may be assumed to be neglectable. Furthermore, both cohorts were imaged using the same standard for propofol use so that no systematic bias should be present. Finally, it would be very interesting to correlate the vascular metrics to other imaging measurements such as tissue perfusion and diffusion changes.

CONCLUSION

The results of this study show that children with MMD/MMS have significantly smaller anterior circulation cerebral vasculature compared with normal controls based on quantitative analyses of MRA data sets. These preliminary results motivate future larger scale studies to validate these morphological parameters as imaging biomarkers for assessing the impact of bypass surgery on disease progression.

Funding

This work is supported in part by the Johns Hopkins Department of Radiology Physician Scientist Incubator Program.

Disclosures

The authors have no personal, financial, or institutional interest in any of the drugs, materials, or devices described in this article.

REFERENCES

1. Mossa-Basha M, Havenon Ad, Becker KJ, et al. Added value of vessel wall magnetic resonance imaging in the differentiation of moyamoya vasculopathies in a non-Asian cohort. *Stroke.* 2016;47(7):1782-1788.
2. Scott RM, Smith ER. Moyamoya disease and moyamoya syndrome. *N Engl J Med.* 2009;360(12):1226-1237.
3. Li J, Jin M, Sun X, et al. Imaging of moyamoya disease and moyamoya syndrome: current status. *J Comput Assist Tomogr.* 2019;43(2):257-263.
4. Quon JL, Mouches P, Kim LH, et al. Age-dependent intracranial artery morphology in healthy children. *Clin Neuroradiol.* 2022;32(1):49-56.
5. Khan N, Lober RM, Ostergren L, et al. Measuring cerebral blood flow in moyamoya angiopathy by quantitative magnetic resonance angiography noninvasive optimal vessel analysis. *Neurosurgery.* 2017;81(6):921-927.
6. Quon JL, Kim LH, MacEachern SJ, et al. Early diffusion magnetic resonance imaging changes in normal-appearing brain in pediatric moyamoya disease. *Neurosurgery.* 2020;86(4):530-537.
7. Goswami P, Markey MK, Warach SJ, Dula AN. Quantitative analysis of the cerebral vasculature on magnetic resonance angiography. *Sci Rep.* 2020;10(1):10227.
8. Bullitt E, Zeng D, Mortamet B, et al. The effects of healthy aging on intracerebral blood vessels visualized by magnetic resonance angiography. *Neurobiol Aging.* 2010;31(2):290-300.
9. MacEachern SJ, Forkert ND. Machine learning for precision medicine. *Genome.* 2021;64(4):416-425.
10. Ratsep MT, Paolozza A, Hickman AF, et al. Brain structural and vascular anatomy is altered in offspring of pre-eclamptic pregnancies: a pilot study. *AJNR Am J Neuroradiol.* 2016;37(5):939-945.
11. Kholmovski EG, Alexander AL, Parker DL. Correction of slab boundary artifact using histogram matching. *J Magn Reson Imaging.* 2002;15(5):610-617.
12. Sled JG, Zijdenbos AP, Evans AC. A nonparametric method for automatic correction of intensity nonuniformity in MRI data. *IEEE Trans Med Imaging.* 1998;17(1):87-97.
13. Forkert ND, Schmidt-Richberg A, Fiehler J, et al. 3D cerebrovascular segmentation combining fuzzy vessel enhancement and level-sets with anisotropic energy weights. *Magn Reson Imaging.* 2013;31(2):262-271.
14. Lee T-C, Kashyap RL, Chu C-N. Building skeleton models via 3D medial surface/axis thinning algorithms. *CVGIP Graph Models Image Process.* 1994;56(6):462-478.
15. Danielsson P-E. Euclidean distance mapping. *Comput Graphics Image Process.* 1980;14(3):227-248.
16. Fonov V, Evans AC, Botteron K, et al. Unbiased average age-appropriate atlases for pediatric studies. *Neuroimage.* 2011;54(1):313-327.
17. Modat M, Cash DM, Daga P, Winston GP, Duncan JS, Ourselin S. Global image registration using a symmetric block-matching approach. *J Med Imaging (Bellingham).* 2014;1(2):024003.
18. Mutsaerts HJ, van Dalen JW, Heijtel DF, et al. Cerebral perfusion measurements in elderly with hypertension using arterial spin labeling. *PLoS One.* 2015;10(8):e0133717.
19. Mouches P, Forkert ND. A statistical atlas of cerebral arteries generated using multi-center MRA datasets from healthy subjects. *Sci Data.* 2019;6(1):29.
20. Alexander MD, de Havenon A, Kim SE, Parker DL, McNally JS. Assessment of quantitative methods for enhancement measurement on vessel wall magnetic resonance imaging evaluation of intracranial atherosclerosis. *Neuroradiology.* 2019;61(6):643-650.
21. Yamada I, Himeno Y, Suzuki S, Matsushima Y. Posterior circulation in moyamoya disease: angiographic study. *Radiology.* 1995;197(1):239-246.
22. Tan C, Duan R, Ye X, Zhang D, Wang R. Posterior Circulation moyamoya disease versus primitive vertebral-basilar artery system moyamoya disease: new classification of moyamoya disease from the perspective of embryology. *World Neurosurg.* 2016;96:222-229.
23. Yamamoto S, Kashiwazaki D, Akioka N, Kuwayama N, Noguchi K, Kuroda S. Progressive shrinkage of involved arteries in parallel with disease progression in moyamoya disease. *World Neurosurg.* 2019;122:e253-e261.
24. Kaku Y, Morioka M, Ohmori Y, et al. Outer-diameter narrowing of the internal carotid and middle cerebral arteries in moyamoya disease detected on 3D constructive interference in steady-state MR image: is arterial constrictive remodeling a major pathogenesis? *Acta Neurochir (Wien).* 2012;154(12):2151-2157.
25. Yuan M, Liu ZQ, Wang ZQ, Li B, Xu LJ, Xiao XL. High-resolution MR imaging of the arterial wall in moyamoya disease. *Neurosci Lett.* 2015;584:77-82.
26. Ryoo S, Cha J, Kim SJ, et al. High-resolution magnetic resonance wall imaging findings of Moyamoya disease. *Stroke.* 2014;45(8):2457-2460.
27. Kim YJ, Lee DH, Kwon JY, et al. High resolution MRI difference between moyamoya disease and intracranial atherosclerosis. *Eur J Neurol.* 2013;20(9):1311-1318.
28. Deng X, Zhang Z, Zhang Y, et al. Comparison of 7.0- and 3.0-T MRI and MRA in ischemic-type moyamoya disease: preliminary experience. *J Neurosurg.* 2016;124(6):1716-1725.
29. Houkin K, Yoshimoto T, Kuroda S, Ishikawa T, Takahashi A, Abe H. Angiographic analysis of moyamoya disease—how does moyamoya disease progress?. *Neurol Med Chir (Tokyo).* 1996;36(11):783-787; discussion 788.
30. Aoyagi M, Fukai N, Yamamoto M, Nakagawa K, Matsushima Y, Yamamoto K. Early development of intimal thickening in superficial temporal arteries in patients with moyamoya disease. *Stroke.* 1996;27(10):1750-1754.
31. Czabanka M, Peña-Tapia P, Schubert GA, Woitzik J, Vajkoczy P, Schmiedek P. Characterization of cortical microvascularization in adult moyamoya disease. *Stroke.* 2008;39(6):1703-1709.
32. Zipfel GJ, Fox DJ Jr, Rivet DJ. Moyamoya disease in adults: the role of cerebral revascularization. *Skull Base.* 2005;15(1):27-41.
33. Kuwabara Y, Ichiya Y, Otsuka M, et al. Cerebral hemodynamic change in the child and the adult with moyamoya disease. *Stroke.* 1990;21(2):272-277.
34. Forkert ND, Li MD, Lober RM, Yeom KW. Gray matter growth is accompanied by increasing blood flow and decreasing apparent diffusion coefficient during childhood. *AJNR Am J Neuroradiol.* 2016;37(9):1738-1744.

COMMENT

The authors of "Intracranial Artery Morphology in Pediatric Moya Moya Disease and Moya Moya Syndrome" begin to aggregate radiographic structural reference data for moyamoya pathology in children. This is useful information in supplementing existing normative data for children. It is reassuring to find that the data suggest a proximal vascular pathology, similar to our overall understanding of moyamoya. This data will be important as the field investigates the mechanisms driving moyamoya.

Furthermore, this manuscript demonstrates exciting progress in the field and highlights new directions. Historically, clinical imaging has been exclusively manually interpreted, which can present a limit in the setting of increasing data volume (both the number of cases, and the number of images for individual patients). Even with the current imaging techniques, there may be patterns in data that are not be fully appreciated. This manuscript is 1 of many reports in increasingly automated or pseudoautomated image analysis techniques, which have both advantages and disadvantages in consistency and novel or complex insights.

Beyond the advances in methodology, the current analysis considers the structural configuration of the vessels, but not the underlying pathophysiology of flow. Although the role of hemodynamics has been described and studied for decades with limited success in guiding brain revascularization surgery, there has been some demonstration of productive clinical guidance by studying normal and abnormal flow. Applying these novel analysis techniques on combined structural and physiological imaging will certainly be the next area of advance in the decision-making of children with moyamoya.

Alfred Pokmeng See
Boston, Massachusetts, USA

Burroughs adding machine. Exhibit in the Ridai Museum of Modern Science, Tokyo University of Science, Kagurazaka campus - 1-3 Kagurazaka, Shinjuku-ku, Tokyo. By Daderot, CC0, via Wikimedia Commons.